Front propagation and mode-locking in an advection-reaction-diffusion system

M. S. Paoletti and T. H. Solomon*

Department of Physics, Bucknell University, Lewisburg, Pennsylvania 17837, USA

(Received 22 May 2005; published 5 October 2005)

Experiments are presented on chemical front propagation in an oscillating chain of vortices in which the mixing of passive impurities is chaotic. The excitable ruthenium-catalyzed Belousov-Zhabotinsky reaction is used in these studies. Velocities of the propagating fronts are measured as a function of the frequency and amplitude of external forcing. Mode locking is observed where the front propagates an integer number of vortices in an integer number of drive periods. Arnol'd tongues are mapped out for two of the locking regimes. These two tongues are shown to form a region of overlap where the velocity of the propagating front switches erratically between two locked values. The experimental results agree with numerical predictions of mode locking in a simplified model of the flow.

I. INTRODUCTION

There is a great deal of interest in the patterns that form in interacting systems; e.g., chemical reactions [1,2], interacting populations and ecosystems [3], and systems undergoing phase transitions [4]. The vast majority of previous research on pattern formation in reacting systems has concentrated on the reaction-diffusion limit [5,6] in which there are no fluid flows; consequently, mixing is achieved solely via molecular diffusion. However, most fluid systems are not stagnant; flows in the system significantly affect the mixing properties and thereby dramatically alter the pattern-formation process. Despite the significant impact fluid mixing has on these processes, there has been very little theoretical work on the more general "advection-reaction-diffusion" problem [7–12], and there have been almost no experimental studies [13–16]. The issue of the role of advection in the pattern-formation process is particularly interesting in light of the discovery that mixing can be *chaotic* even for very simple, laminar fluid flows [17,18].

Many reacting systems are characterized by the propagation of a front across the system. Examples of front propagation can be seen in a wide range of systems, such as marine ecology [19,20], combustion [21,22], solidification [4], and the spreading of diseases [23]. The majority of previous studies of front propagation deal with the reaction-diffusion regime. The effects of fluid flows on front propagation, by contrast, have not been studied in great detail. In particular, a greater understanding of the role of coherent flow structures—such as vortices—on the front propagation process is needed.

In this article, we present experimental studies of chemical front propagation in an advection-reaction-diffusion system. A variation of the excitable Ruthenium-catalyzed Belousov-Zhabotinsky reaction is used to generate a chemical pulse which can be manipulated (and, in fact, erased) optically. The flow consists of a chain of alternating vortices in an annular configuration. The system is forced periodi-

cally with the vortex chain oscillating in the azimuthal direction, resulting in chaotic mixing [24–26]. In the experiments presented here, the velocities of the chemical fronts are studied as a function of the amplitude and frequency of the external forcing. The experimental results are compared to previous numerical studies [11] that predict mode locking of the chemical fronts to the external forcing. Mode-locking behavior has been seen in many other physical systems [27,28]; this, however, is the first experimental evidence of mode locking in an advection-reaction-diffusion system [16].

In Sec. II we present a summary of theories and numerical simulations that are relevant to the current experiments. Section III provides details on the experimental techniques, chemical reaction used in these experiments, and analysis techniques. The experimental results are presented in Sec. IV and further discussed in Sec. V.

II. BACKGROUND

A. Front propagation

A wide range of front propagation processes can be modelled by autocatalytic reactions of the form $A+B \rightarrow 2B$ [12]. This corresponds to the case where a stable phase (B) penetrates into an unstable phase (A). The dynamics of a propagating front is governed by the interplay between mixing in the system and the interaction between the different species. For an autocatalytic process in the reaction-diffusion limit the front speeds depend upon the molecular diffusivity D_0 and the production process of the reaction that occurs on a time scale τ. In the absence of fluid flows, the front velocity v_0 has been predicted by Fisher and Kolmogorov [29–31] to be given by

$$v_0 = 2\sqrt{\frac{D_0}{\tau}}. \tag{1}$$

Although derived specifically for autocatalytic processes, this result has also been shown to hold for certain "trigger" or pulselike reactions, including the Ru-catalyzed BZ reaction used in these experiments [32].

The next question is as follows: how is the front velocity modified in the presence of fluid flows? In general the front

*Email address: tsolomon@bucknell.edu

FIG. 1. Schematic of a chain of alternating vortices. The arrows show the direction of the flow within each vortex.

velocity will not be constant; however, it is reasonable to expect that it will be possible to define an average velocity v_f that can be predicted theoretically from the generalized advection-reaction-diffusion problem. This average front velocity v_f is bounded above by $v_0 + U$, where U is the maximum flow velocity.

Transport in many fluid flows can be characterized as enhanced diffusion with an effective diffusion coefficient D_{eff}. It is natural to propose that the Fisher-Kolmogorov theory might still apply for these cases, assuming the molecular diffusion coefficient D_0 in Eq. (1) is replaced by the effective diffusion coefficient D_{eff}. In the limit of very slow reaction [21], this approach works, since the advection in the system dominates the dynamics [33]. Similarly, in the limit of very *fast* reactions, the flow becomes insignificant and the Fisher-Kolmogorov result is valid. For typical, naturally occurring systems, however, the reaction time scale τ is often on the order of the fluid velocity time scale. In this case replacing D_0 with D_{eff} is insufficient [34].

A general method for theoretically predicting v_f for advection-reaction-diffusion systems is still unknown and therefore numerical simulations must be employed. The dynamics of such fronts is simulated in the geometrical optics regime [35] by Cencini *et al.* [11]. The geometrical optics regime corresponds to the limit of fast reaction and thin fronts, and is rigorously defined as the limit of $\tau \rightarrow 0$ and $D_0 \rightarrow 0$ while maintaining the ratio D_0/τ constant [36].

B. Oscillating vortex chain

The flow in these studies is an oscillating vortex chain, as shown in Fig. 1. Time dependence is achieved by oscillating the entire chain periodically in a lateral direction (along the direction of the chain). This flow has been modeled numerically [24] using the following stream function:

$$\psi(x,y,t) = \frac{U}{k} \sin[kx_s(t)]W(y), \quad (2)$$

where $x_s(t) = x + B \sin(\omega t)$ accounts for the lateral oscillation of the vortex chain with amplitude B and angular frequency ω. The x and y velocities for tracers moving in the flow can be derived from Eq. (2) via Hamilton's equations of motion $\dot{x} = \partial\psi/\partial y$ and $\dot{y} = -\partial\psi/\partial x$. The y dependence $W(y)$ is determined by the boundary conditions at $y=0$ and $y=d$. For free-slip boundary conditions

$$W(y) = \sin(\pi y/d). \quad (3)$$

The resulting flow is modeled by the following equations:

$$u_x(x,y,t) = U \sin\left(\frac{\pi}{d}[x + B\sin(\omega t)]\right)\cos\left(\frac{\pi}{d}y\right), \quad (4)$$

$$u_y(x,y,t) = -U \cos\left(\frac{\pi}{d}[x + B\sin(\omega t)]\right)\sin\left(\frac{\pi}{d}y\right), \quad (5)$$

where u_x and u_y are the flow velocities in the x and y directions, respectively, U is the maximum flow velocity, and d is the width and height of a vortex. The y dependence is more complicated for the case with no-slip boundary conditions [37].

The vortices in these studies have unity aspect ratio; the wavelength (which is two vortex widths) is $\lambda = 2d$. The oscillation amplitude can be expressed nondimensionally as a fraction of a vortex width $b \equiv kB/\pi$, where k is the wave number defined as $k = 2\pi/\lambda$. The oscillation frequency may be scaled by the advective (mixing) time scale $\tau_{\text{adv}} \equiv 2\pi/kU$. By using this time scale, the frequency of oscillation can be expressed nondimensionally by $\nu \equiv \omega/kU$.

Mixing in the oscillating vortex chain depends critically on the oscillation amplitude b. If $b=0$ then the vortex chain is stationary (time-independent). In this regime, long range mixing is slow, determined by an interplay between advection of impurites within the vortices and diffusion across the separatrices from one vortex to the next [38,39]. For $b \neq 0$, the resulting time dependence produces chaotic mixing [24,25,40–42] which greatly enhances long-range transport. For small oscillation amplitudes, tracers near the centers of the vortices typically follow ordered trajectories, while those near the perimeters of the vortices follow chaotic trajectories. The size of the chaotic region around and between the vortices grows with oscillation amplitude; in fact, for many of the experimental runs, the chaotic region occupies a significant portion of the flow.

C. Mode locking and Arnol'd tongues

Mode locking can occur for a system that is periodically forced by an external stimulus. Systems that mode-lock typically have a natural, internal frequency of oscillation in the absence of external forcing. Mode locking occurs when the system changes its natural frequency to become a rational multiple of the frequency of the external stimulus. Mode-locking phenomenon has been seen in a wide range of physical, chemical, and biological systems. Examples include circadian rhythms (24-h periodicity) such as the sleep-wake cycles forced by the sun [43], arrays of Josephson's junctions [44], and chemical oscillators [45].

Mode-locking behavior has been shown to depend both upon the frequency of the imposed forcing as well as the amplitude. Ideally, for frequencies very near the natural frequency of oscillation for the system, only small oscillation amplitudes should be required to induce mode locking. Further from the natural frequency, though, greater amplitudes are required to cause the system to change its oscillation frequency to match that of the external forcing. Typically, threshold amplitudes exist below which the system will not mode lock for any frequency.

The dependence of mode-locking behavior on both the frequency and amplitude of oscillation is shown by mapping out "Arnol'd tongues" [46] for a given system. Arnol'd tongues are represented by plotting a parameter-space diagram (amplitude versus frequency) showing locking behavior. An Arnol'd tongue is the region in this parameter space in which the system is mode locked with a particular (rational) ratio of the internal and external frequencies.

D. Simulations of mode locking in front propagation

The propagation of a reacting front has been simulated numerically for the oscillating vortex chain by Cencini *et al.* [11] and by Abel *et al.* [9,10]. The simulations assume an autocatalytic ("burn") reaction where the reactants are consumed, similar to a flame consuming fuel. Those studies assume that in the absence of any fluid flow the reacting front will propagate with a constant velocity v_0, as discussed in Sec. II A. The numerical algorithm presented in Ref. [11] combines a spreading reaction front with the oscillating vortex chain flow of Eqs. (4) and (5). We have reproduced these simulations ourselves for comparison with the experiments.

For the stationary vortex chain ($b=0$), mixing between adjacent vortices is limited by molecular diffusion. Therefore, the propagation of the front from one vortex to the next is solely by a reaction-diffusion mechanism. However, within a vortex the front propagation is dominated by advection. As the maximum flow velocity increases, the front velocity also increases since the time to travel around a given vortex decreases. The result is a monotonic increase in the front velocity as the maximum flow velocity increases [11].

For an oscillating vortex chain ($b \neq 0$), mixing between vortices is chaotic. Cencini *et al.* study the velocities of the propagating fronts as a function of the oscillation frequency for a particular oscillation amplitude. Mode-locking behavior is found for particular ranges of frequencies. Mode locking in this system is defined as the front propagating an integer number N of wavelengths λ of the flow (2 vortex widths) in an integer number M of oscillation periods τ. Consequently, the velocity v_f for the mode-locked fronts is given by

$$v_f = \frac{N}{M}\frac{\lambda}{\tau}. \qquad (6)$$

Equation (6) can be rewritten as

$$v_f = \frac{N}{M}\lambda f \qquad (7)$$

or, nondimensionally as

$$\xi = \frac{N}{M}\nu, \qquad (8)$$

where $\xi \equiv v_f/U$.

For a (1,1) mode lock (that is $N=1$, $M=1$), the shape of the reaction front repeats every period of oscillation and is rigidly translated by λ, one wavelength of the flow. A sequence of numerical images for a (1,1) mode lock is shown in Fig. 2. For a (1,2) mode lock (Fig. 3), the shape of the front repeats every 2 drive periods. In this case, it also takes
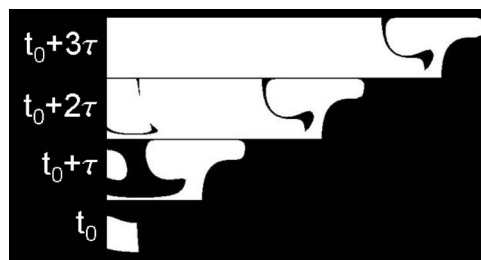

FIG. 2. Simulation showing evidence for a (1,1) mode lock. A snapshot of the reacting front is taken at some intial time t_0. Another snapshot is taken after each period τ of the oscillation. The shape of the reacting front repeats every period and is rigidly translated by λ after a transient, as expected for a (1,1) mode lock. The parameters used in this simulation are $b=0.3$, $f=0.5$, $U=1.0$, and $v_0=0.2$.

two drive periods for the front to advance one wavelength of the flow.

A more rigorous test of mode locking can be obtained by plotting the front velocity as a function of the external frequency and comparing the results to the the predictions of Eq. (8). This has been done by Cencini *et al.* for a particular oscillation amplitude (see Fig. 11 in Ref. [11]). Clear mode locking is found in these simulations for the (1,1), (1,2), (1,4), and (1,6) locking branches, with front velocities in agreement with Eq. (8) for a wide range of frequencies.

Note that mode locking of the propagating front is inconsistent with the Fisher-Kolmogorov prediction [Eq. (1)] for reaction-diffusion systems, even with an enhanced diffusion coefficient.

III. EXPERIMENTAL TECHNIQUES

A. Apparatus and flow

The alternating vortex chain—composed of 20 vortices (10 wavelengths)—is produced using a magnetohydrodynamic technique [16,25,47,48] shown in Fig. 4. A radial current passes through a 2-mm-thick solution and interacts with a spatially varying magnetic field. The magnetic field is produced by two concentric rings of magnets of alternating polarity, where the polarity alternates both in the azimuthal as well as the radial direction. For a radial current, magnetic
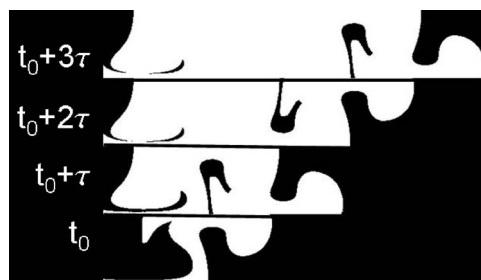

FIG. 3. Simulation showing evidence for a (1,2) mode lock. The shape of the reacting front repeats every other period and is rigidly translated by λ every two periods after a transient, as expected for a (1,2) mode lock. The parameters used in this simulation are $b=0.3$, $f=1.0$, $U=1.0$, and $v_0=0.2$.
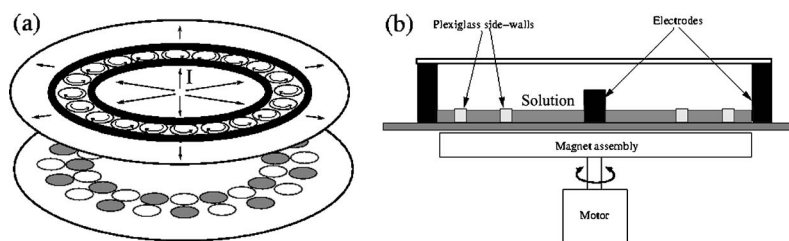
FIG. 4. Schematic of the flow and experimental apparatus. (a) Exploded view of the magnetohydrodynamic forcing technique. The flow is an annular vortex chain bounded by two plexiglass rings (shown in black) with radii 6.1 and 8.3 cm. (b) Side view of the apparatus. A circular container holds the fluid and the bounding rings. Below the container is the magnet assembly, which is mounted coaxially with a motor.

forcing pushes the fluid azimuthally above the magnets, one way above magnets with the north side up and the opposite way above magnets with the south side up. Plexiglass bounding rings of radius 6.1 and 8.3 cm form the boundaries of the region of interest, which is an annulus for these experiments. By using the magnet array and bounding rings shown in Fig. 4, the resulting flow is an annular chain of vortices. The strength of the flow—characterized by the maximum flow velocity U—is varied by changing the magnitude of the electrical current passing through the fluid. Unless otherwise stated, $U=440$ μm/s for all of the experiments.

The magnet array is mounted coaxially on a motor that can be programmed to move with any arbitrary, input wave form. A stationary vortex chain is produced by having the motor off. An oscillating vortex chain is produced by having the magnets oscillate with a specified frequency f and amplitude B.

The experimental flow differs from the model of Eqs. (4) and (5) in a few respects. First, the model flow assumes free-slip rather than the no-slip boundary conditions that are present at the bounding walls and bottom of the container. Second, there is a weak, secondary, three-dimensional flow that slowly pumps fluid into and up through the center of each vortex [47]. The model equations assume a two-dimensional flow, whereas the secondary flow present within the experiments makes the experimental flow weakly three dimensional. Third, the experimental vortex chain is wrapped around into an annulus; consequently, there are some curvature effects that are absent in the model. Fourth, there are presumably some weak flows that are induced by the chemical reaction itself, as has been predicted in previous studies [49]. Our expectation is that these induced flows are significantly smaller than the flows forced by the MHD technique.
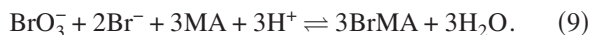
B. Reaction

A variation of the Belousov-Zhabotinsky (BZ) reaction [50,51] is used in the experiments presented here. Rather than the standard ferroin-catalyzed BZ reaction, the ruthenium-catalyzed BZ reaction is used. The Ru-catalyzed BZ reaction may be either oscillatory [52] or excitable [32,53], depending on the reactant concentrations. The oscillatory reaction oscillates between the Ru^{2+} state, which is orange in color, and the Ru^{3+} state which is green.

The excitable regime of the reaction is used in these experiments. The system begins completely in the stable Ru^{2+} state. A Ru^{3+} pulse may then be triggered by placing a thin (0.25 mm) silver wire into the solution for approximately ten seconds. The silver oxidizes the Ru^{2+} in the vicinity of the wire to the Ru^{3+} state. This region of Ru^{3+} then triggers the surrounding Ru^{2+} and so forth, resulting in the propagation of a Ru^{3+} front across the system. The reaction propagates as a pulse rather than as a burn; the region behind the chemical front returns to the Ru^{2+} state and may be retriggered. (In fact, due to recirculation in the flow, the region behind the front is repeatedly retriggered after the initial pulse passes.) The dynamics of the front edge of the pulse is assumed to be the same as the dynamics of the leading edge of a burn front. Therefore, the excitable Ru-catalyzed BZ reaction may be used to produce a propagating front in an advection-reaction-diffusion system, as desired.

Another advantage of the Ru-catalyzed BZ reaction is the fact that it is photosensitive for both the oscillatory and excitable regimes [52]. The photosensitivity of the reaction allows for the dynamics to be manipulated by light. For example, by shining sufficiently intense blue light on the reaction, the oscillatory behavior can be stifled leaving the reaction entirely in the Ru^{2+} state. Examples of both pattern formation [54] and mode locking [45] in a reaction-diffusion regime have been produced using photoinhibition for the oscillatory regime of the reaction.

The ruthenium indicator used in these experiments comes in the $[\text{Ru(bpy)}_3]\text{Cl}_2 6\text{H}_2\text{O}$ form. The Cl$^-$ ions inhibit the reaction and also decrease the photosensitivity; therefore, the Cl$^-$ ions should be removed before the experiment is run. To remove the Cl$^-$ ions, a single-replacement reaction is used [57]. The bromomalonic acid (BrMA) used in these experiments is produced before each run by the following reaction [53]:

$$\text{BrO}_3^- + 2\text{Br}^- + 3\text{MA} + 3\text{H}^+ \rightleftharpoons 3\text{BrMA} + 3\text{H}_2\text{O}. \quad (9)$$

The reaction must be performed in a fume hood.

For most of the experiments in this paper, the initial concentrations are as follows: $[\text{BrMA}]=0.09$ M, $[\text{H}_2\text{SO}_4]=0.28$ M, $[\text{BrO}_3^-]=0.16$ M, $[\text{MA}]=0.03$ M, $[\text{Ru(bpy)}_3^{2+}]=2.7$ mM. The solution is initially orange in color and remains orange until a silver wire is placed in the solution, triggering the pulse. For these experiments, the reaction-diffusion (no-flow) front velocity is $v_0=52$ μm/sec.

A variation of the Ru-catalyzed BZ reaction with enhanced photosensitivity is used for experiments in which the chemical front propagates around the annulus more than once ("wrap around"). In order to do so, the tail of the reacting front is reduced back to the Ru^{2+} ("erased") using photoinhibition, which is further explained in the next section. To increase the photosensitivity the sulfuric acid concentration $[H_2SO_4]$ is decreased from 0.28 M to 0.22 M; all other chemical concentrations are the same as those mentioned above. It should be noted that the more photosensitive combination could have been used for all of the data runs. The wrap-around experiments were done last, however; consequently, most of the data had already been obtained with the higher H_2SO_4 concentration. More details about the reaction and the methods used to prepare the chemicals can be found in Ref. [55].

C. Illumination and imaging techniques

To exploit the photosensitivity of the Ru-catalyzed BZ reaction, a high-powered (205 W) video projector is used to illuminate a pattern onto the system. The annular region of interest is illuminated with red light which does not affect the reaction dynamics. Furthermore, the Ru^{3+} state strongly absorbs light at 675.2 nm whereas the Ru^{2+} does not, so the use of red light greatly improves image contrast. The rest of the circular container is illuminated with blue and green light, which inhibits the reaction [52], thereby preventing any spurious fronts from entering the region of interest.

Within the annular region, one to two vortices are also illuminated with blue and green light to form a "blinding region." Since the reaction is inhibited by blue light, the reaction front cannot pass through the blinding region. Therefore, by triggering a chemical pulse next to the blinding region, the chemical front can travel in only one direction around the annulus. Then, instead of having only 10 vortices of data if the reaction front were to travel in both directions and meet itself halfway around the annulus, the front traverses 18–19 vortices.

To obtain even more than 19 vortices of data, a wrap-around approach is used. This approach uses the enhanced photosensitivity discussed in the previous section and a dynamic blinding region that follows the advancing chemical front. The blinding region is extended to cover nearly half of the annulus while the other half is still illuminated with red light. A chemical pulse is triggered within the red region, and as the front advances the blinding region follows it in a way such that the leading edge of the front always remains approximately in the center of the red region. (The blinding region is always kept at least three vortices away from the leading edge of the front.) As a result, the tail of the chemical pulse is erased (the Ru^{3+} state is reduced back to the initial Ru^{2+} state) by the illumination, allowing the front to propagate around the annulus multiple times.

Images of the propagating front are captured using a 12-bit, high resolution CCD camera. Unless otherwise stated, the time-interval between images in all the experiments presented here is 2.0 s. A red interference filter (676 nm), which only passes light from 674–678 nm, is placed over the lens
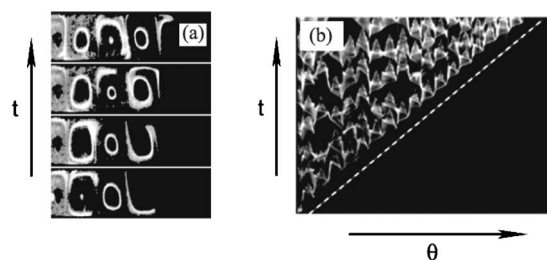

FIG. 5. Propagation of a Ru^{3+} pulse for the stationary ($b=0$) vortex chain. (a) Time series of the propagating front; images are separated in time by 32 s. (b) Corresponding space-time plot, obtained by stacking radially summed and decurled images. The dashed line shows the average velocity of the front.

of the camera to improve image contrast. The Ru^{3+} state strongly absorbs light at 675.2 nm and can therefore easily be distinguished from the Ru^{2+} state with this particular filter.

D. Analysis

The velocity of the chemical front is determined from the sequence of images. The first image taken is used as a background image and the intensity of each subsequent image is subtracted from this background. The images are subtracted from the background since the Ru^{3+} is dark due to the interference filter used. As a result, once subtracted, the Ru^{3+} front appears white in the subtracted images.

Each of the subtracted annular images is "decurled" thereby displaying the annular vortex chain as a linear vortex chain. The horizontal axis of the decurled images corresponds to the azimuthal direction of the annulus and the vertical direction corresponds to the radial direction. Since the region of interest is an annulus, if the front leaves the right edge of the decurled image it will appear at the left edge and continue propagating to the right.

Each decurled image is then shifted by the same amount in the azimuthal direction such that the front is triggered at $\theta=0$ for each run. The intensity of each image is summed in the radial direction and stacked one on top of another to make a space-time plot, as shown in Fig. 5(b), for example. The velocity of the front is the inverse slope of the leading edge in the space-time plot.

IV. EXPERIMENTAL RESULTS

A. Stationary vortex chain

The time evolution of the reacting front in the stationary vortex chain ($b=0$) is shown in Fig. 5. In the time-independent case, the front advances by three primary mechanisms. (1) Once initiated near a fixed point at the corner of a given vortex, the front is predominantly advected around the perimeter of the vortex. (2) Once the front has reached the opposing corner of the vortex, the front travels across the separatrix via reaction diffusion and triggers a reaction within the next vortex. (3) Having advected around the perimeter of a vortex, the front also travels inward to the center of the vortex via reaction diffusion. Advection around the vortex (1) is rapid, while reaction (2) across the separa-
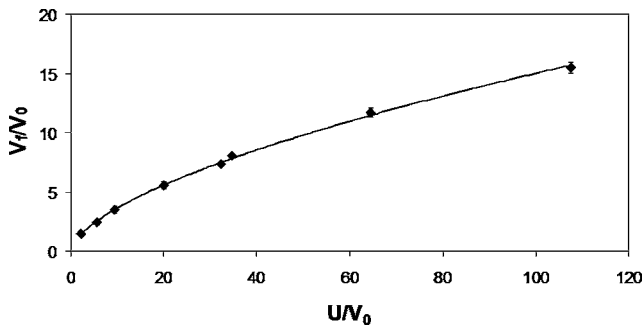
FIG. 6. Experimental plot of the average front velocity v_f as a function of the maximum flow velocity U for the stationary ($b=0$) vortex chain; both velocities are normalized by the reaction-diffusion (no flow) front velocity v_0. The line of best fit has a functional form $v_f/v_0=0.87(U/v_0)^{0.62}$.

trix is slow, resulting in speeding up and slowing down of the front within each vortex [seen as the "teeth" in the spacetime plot, Fig. 5(b)]. The process repeats itself every wavelength of the flow; the result is a velocity that is constant over distances greater than a vortex width.

The front velocity v_f increases monotonically with the maximum flow velocity U (Fig. 6). This can be explained from the fact that the time for a front to advect around a vortex drops with increasing U. However, the relation is not linear. This is due to the fact that propagation from one vortex to the next is limited by the reaction-diffusion mechanism, since there is no advection directly from one vortex to the next. Furthermore, there is a limit on the values of U for which v_f is even defined; as U grows too high, the reaction is extinguished due to the increased shearing. The specifics of this limit have not been extensively studied as of yet but have been qualitatively observed.

B. Mode locking in the oscillating vortex chain

The behavior for the oscillating vortex chain ($b \neq 0$) [Figs. 7(a), 8(a), and 9(a)] is dominated by chaotic advection and can be quite different from the stationary case [Fig. 5(a)]. The stretching and folding that is characteristic of cha-
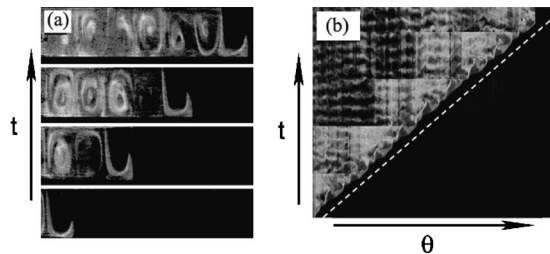

FIG. 7. Experimental evidence for a (1,1) mode-locked front in the oscillating vortex chain ($\nu=0.2255$ and $b=0.345$). (a) A time series showing the propagation of the front. Each image is separated in time by one oscillation period ($\tau=190$ s). The shape of the front repeats every oscillation period and is rigidly translated by one wavelength (two vortices). (b) Corresponding space-time plot. The dashed line shows the constant velocity of the front and agrees with Eq. (8).
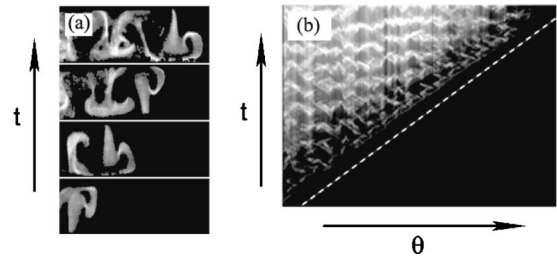

FIG. 8. Experimental evidence for a (1,2) mode-locked front in the oscillating vortex chain ($\nu=0.54$ and $b=0.345$). (a) A time series showing the propagation of the front. Each image is separated in time by one oscillation period ($\tau=80$ s). The shape of the front repeats every other oscillation period and is rigidly translated by one wavelength (two vortices) every two periods. (b) Corresponding space-time plot. The dashed line shows the constant velocity of the front and agrees with Eq. (8).

otic mixing of passive impurities [25,26] can be seen in the advection-reaction-diffusion images presented here. Evidence for mode locking can be seen by examining a time series of snapshots of the chemical front separated by one period of oscillation. An example of mode locking with $(N,M)=(1,1)$ is shown in Fig. 7(a). Similar to the simulation shown in Fig. 2, the shape of the leading edge of the front is repeated and rigidly translated by one wavelength every period of oscillation. The corresponding space-time plot is shown in Fig. 7(b). There is a very clear, constant velocity throughout the duration of the run, consistent with the prediction of Eq. (8).

An example of a (1,2) mode lock is shown in in Fig. 8(a). Similar to the simulation shown in Fig. 3, the shape of the leading edge is repeated and rigidly translated by one wavelength every two periods. The corresponding space-time plot for this run is shown in Fig. 8(b). Once again, the leading edge of the front propagates at a constant velocity.

An example of an unlocked case is shown in Fig. 9(a). The time series for this case does not show the repeating translation seen in Figs. 7(a) or 8(a). Furthermore, there is no clear, single velocity for this frequency; the space-time plot [Fig. 9(b)] has many undulations and the velocity is continually changing. It could be argued that this frequency may simply fall on a locking branch that is inaccessible due to the fact that only twenty vortices are used. However, comparison
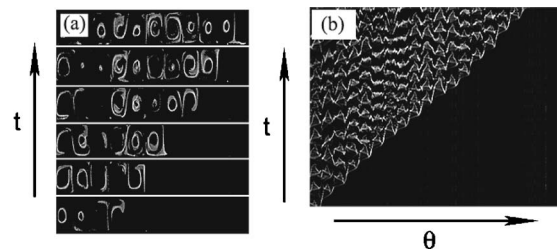

FIG. 9. Experimental evidence for an unlocked front in the oscillating vortex chain ($\nu=0.3296$ and $b=0.086$). (a) A time series showing the propagation of the front. Each image is separated in time by one oscillation period ($\tau=130$ s). The shape of the front does not repeat. (b) Corresponding space-time plot. There is no constant velocity that agrees with Eq. (8).
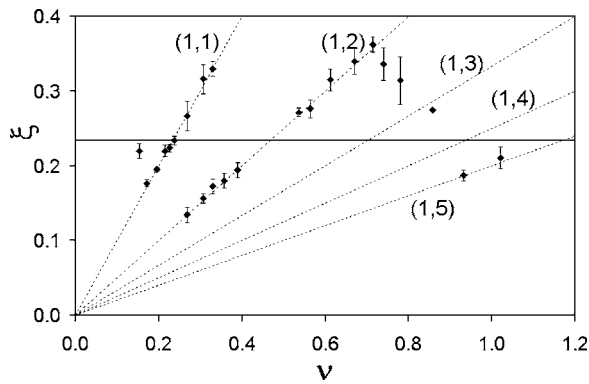
FIG. 10. Front propagation velocities for the oscillating vortex chain; $b=0.345$. The velocity for the stationary case (see Fig. 5) is denoted by the horizontal line. The dashed, diagonal lines correspond to the predictions from Eq. (8) for mode-locked fronts with integers (N,M).

FIG. 11. Arnol'd tongues for the mode-locked regimes; □ and ○ correspond to locking with $(N,M)=(1,1)$ and $(1,2)$, respectively; △ corresponds to dual-locked states; $+$ and $\times$ denote partially locked runs; and solid diamond corresponds to unlocked fronts. The dotted and dashed curves show roughly the boundaries of the $(1,1)$ and $(1,2)$ tongues, respectively.

of this run with those at very close frequencies reveals no linear scaling of the front velocity with frequency [see Eq. (8)] another typical indication of mode locking that is absent.

To test predictions of mode-locking in the oscillating vortex chain, a particular amplitude of oscillation is chosen ($b=0.345$) and the nondimensionalized front velocity ξ is plotted as a function of the nondimensionalized frequency ν for this amplitude (Fig. 10). The dashed lines correspond to the theoretical predictions of Eq. (8). The solid, horizontal line corresponds to the stationary velocity (for $b=0$) measured for the same value of U. There are clearly many frequencies that mode lock onto both the $(1,1)$ and $(1,2)$ locking branches and a couple on the $(1,5)$ locking branch. It should be noted that there are no fitted parameters in this plot.

The plot of ξ versus ν shown in Fig. 10 does not capture the full advection-reaction-diffusion problem. The maximum flow velocity U and the oscillation frequency f could both be doubled, for instance, leaving the advective properties of the flow (represented by the non-dimensional frequency ν) the same. However, it would take only half the time to achieve the same amount of mixing, but the reaction time scale would remain unchanged. Consequently, the balance between advection, reaction and diffusion would be altered, potentially resulting in different dynamics. As an extreme example, for $U\rightarrow\infty$, the system becomes an advection-diffusion system and the dynamics of the reaction is lost. For $U\rightarrow0$, the system becomes a reaction-diffusion system and the effects of the fluid flows are lost and the front will propagate at velocity v_0.

C. Arnol'd tongues

Although the mode-locked front velocity is fully determined by the oscillation frequency, whether the system mode locks or not is also dependent upon the oscillation amplitude. As the oscillation amplitude approaches zero, all front velocities will tend toward the stationary velocity rather than the predicted, locked velocity. Therefore, the range of frequencies that will mode lock on a particular branch ought to decrease with decreasing oscillation amplitude, resulting in Arnol'd tongue behavior.
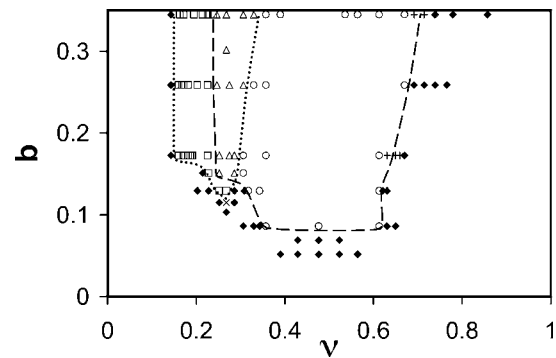
Arnol'd tongues for our experiments are shown in Fig. 11 for the $(1,1)$ and $(1,2)$ locking regimes. Several types of behavior are displayed within this plot. Most simply are the cases where the front either mode-locks onto the $(1,1)$ or $(1,2)$ branches symbolized by □ and ○, respectively, or is completely unlocked (filled in diamonds). Near the edges of the tongues the front may be "partially locked," defined as the front being locked for 25–75 % of the total run. These partially locked cases are denoted by $+$ and $\times$ for the $(1,1)$ and $(1,2)$ tongues, respectively.

The mode-locking behavior shows a clear dependence upon the oscillation amplitude. As the oscillation amplitude increases, the range of frequencies over which the system mode-locks increases. Furthermore, as the oscillation amplitude decreases towards zero, the system does not lock for any frequencies of oscillation, as expected. Specifically, no mode-locking behavior is observed for amplitudes below $b=0.075$.

D. Overlapping Arnol'd tongues

The $(1,1)$ and the $(1,2)$ tongues overlap for a large range of amplitudes, denoted by △ in Fig. 11. The overlap can also been seen in Fig. 10; specifically, the front velocity ξ is not single-valued for all frequencies. Within this overlap region dual-locked behavior occurs. The front velocity switches alternately (and erratically) between two different values, corresponding to the two different locking tongues. In these cases, both velocities are plotted in Fig. 10.

To explore the switching behavior between the overlapping Arnol'd tongues the wrap-around technique is used, allowing for the front to travel significantly farther than the 20 vortices available in one transit around the annulus. In addition to increasing the photosensitivity (see Sec. III B), the maximum flow rate is tripled in order to allow for the chemical front to travel around the annulus more than once before the chemicals are exhausted. This is achieved by increasing the maximum flow velocity to $U=1.32$ mm/sec, rather than $U=440$ μm/sec. Because of the faster flow, the interval between acquisition of images is reduced to 1.0 s.
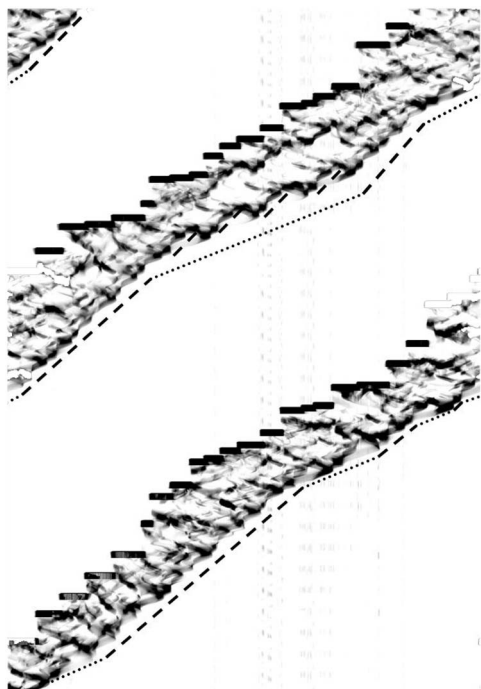
FIG. 12. Space-time plot showing switching behavior between the (1,1) and (1,2) locking tongues; $\nu=0.2465$ with $U=1.32$ mm/s and $b=0.40$. The wrap-around technique is used in this run. The dotted line shows regions for which the front propagates at a velocity corresponding to mode locking with $(N,M)=(1,1)$. The dashed lines show mode locking for $(N,M)=(1,2)$.

Unlocked, single-locked and dual-locked cases are all observed for wrap-around experiments. A space-time plot for a dual-locked case is shown in Fig. 12. The front spontaneously switches a total of 11 times between the (1,1) and (1,2) locking branches. Furthermore, there are times when the front is simultaneously locked on both the (1,1) and (1,2) locking branches. A sequence of images for this run (Fig. 13) shows this simultaneous dual locking. The front begins locked on the (1,2) tongue. However, along the outside of the annulus (bottom of each image), a thin portion of the front is able to shoot ahead of the rest of the front. This thin filament is the portion of the front that is mode locked on the (1,1) branch, evidenced by a fast front velocity that is measured to agree with Eq. (8). The portion of the front that remains behind, however, follows the behavior corresponding to the (1,2) mode. The result is the split in the front as shown in the topmost image. Ultimately, the filament that shoots ahead burns its way into the vortex centers, so the (1,1) mode dominates in the long term during these simultaneous regimes.

Note that on the second trip around the annulus the front does not follow the same switching pattern as it does the first time (Fig. 12). Therefore, the cause of the switching is not governed by the location within the apparatus.

There have been theoretical predictions of chaotic switching when there are overlapping Arnol'd tongues [56]. However, to experimentally verify the chaotic nature of this switching, many more switches are required within a single run. Therefore, in order to perform the analysis, the reaction
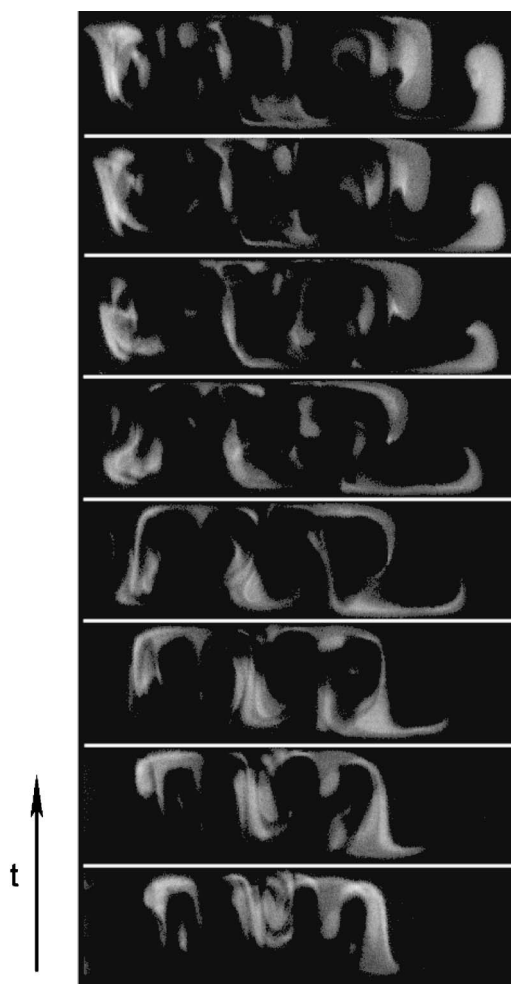

FIG. 13. Sequence of images showing the simultaneous existence of mode-locking on the (1,1) and (1,2) tongues as shown in Fig. 12 for $\nu=0.2465$ with $U=1.32$ mm/s and $b=0.40$. The images are separated in time by 5 s.

would have to be able to last several more hours in order to obtain the necessary data. This could be achieved in future experiments by refreshing the reactants during the run. In conjunction with the wrap-around illumination technique, arbitrarily long runs could be achieved.

V. DISCUSSION

The experimental results presented here agree with the previous numerical studies [11], despite the differences between the model and experimental flows (see Sec. III A). In addition to the differences in the flows, the simulations also assume a burn reaction whereas the experiment produces a pulse reaction. Lastly, the mode-locking behavior is unaffected by the wrap-around technique, even though the chemistry changes over time. From all of this, we can conclude that the mode-locking phenomenon is quite robust.

The behavior shown in these experiments is similar to mode locking and Arnol'd tongue behavior in other systems. However, in other examples of mode locking, there is typically a well-defined, global, natural frequency of oscillation

for the system. In those cases, it is this internal frequency of oscillation that changes to lock onto the imposed, external forcing. In the advection-reaction-diffusion experiments presented here, there is no well-defined, internal frequency of oscillation. The closest analog in this system to a natural, internal frequency is the typical circulation frequency within a vortex. This frequency, though, is dependent on the location within the vortex and diverges for tracers moving along the separatrices. Furthermore, the circulation frequency is independent of whether the chemical front locks or not. It is the reaction itself—the propagating front—that locks onto the external frequency.

The experimental results illustrate the need to go beyond the Fisher-Kolmogorov theory for describing front propagation in generalized advection-reaction-diffusion systems. Even though transport in this system is diffusive with an enhanced diffusivity D_{eff}, the results presented here cannot be obtained from Eq. (1) with D_0 replaced by D_{eff}. Clearly the cellular structure of the flow plays an important role in this process. We expect this to be a general result—the presence of coherent structures in a flow should be expected to have a significant effect on the motion of fronts. The importance of this result goes beyond situations with laminar flows, as coherent structures are prevalent in a wide range of flows, including turbulent flows that are often characterized by the formation of large, persistent patches of vorticity.

The fact that the transport within the system is dominated by chaotic advection raises another interesting question. For many of the mode-locked cases, trajectories of fluid elements within the flow are predominately chaotic. Despite the chaotic nature of the mixing, the overall behavior of the spreading reaction when mode locked is time periodic as shown in Figs. 7(a) and 8(a). This might not seem surprising at first, since the velocity field itself is periodic. But from a chemistry perspective, it is not the velocity *field* that is important but rather the manner in which the chemicals are mixed, and the mixing is clearly chaotic in this system.

Ultimately, a deeper theoretical understanding is needed to explain the locking behavior seen in these experiments. In particular, the question arises as to whether some of the theoretical tools used to describe chaotic mixing can be applied toward explaining the mode-locking behavior.

ACKNOWLEDGMENTS

[1] A. T. Winfree, Science **175**, 634 (1972).

[2] K. Showalter, J. Chem. Phys. **73**, 3735 (1980).

[3] R. S. Cantrell, SIAM Rev. **38**, 256 (1996).

[4] *Handbook of Crystal Growth*, edited by D. T. J. Hurle (North-Holland, Amsterdam, 1993), Vol. 1B.

[5] P. Grindrod, *The Theory and Applications of Reaction-diffusion Equations: Patterns and Waves* (Clarendon Press, Oxford, 1996).

[6] D. Ben-Avraham and S. Havlin, *Diffusion and Reactions in Fractals and Disordered Systems* (Cambridge University Press, Cambridge, 2000).

[7] Z. Neufeld, I. Z. Kiss, C. S. Zhou, and J. Kurths, Phys. Rev. Lett. **91**, 084101 (2003).

[8] I. Scheuring, G. Karolyi, T. T. A. Pentek, and Z. Toroczkai, Freshwater Biol. **45**, 123 (2000).

[9] M. Abel, A. Celani, D. Vergni, and A. Vulpiani, Phys. Rev. E **64**, 046307 (2001).

[10] M. Abel, M. Cencini, D. Vergni, and A. Vulpiani, Chaos **12**, 481 (2002).

[11] M. Cencini, A. Torcini, D. Vergni, and A. Vulpiani, Phys. Fluids **15**, 679 (2003).

[12] T. Tel, A. de Moura, C. Grebogi, and G. Karolyi, Phys. Rep. **413**, 91 (2005).

[13] P. D. Ronney, B. D. Haslam, and N. O. Rhys, Phys. Rev. Lett. **74**, 3804 (1995).

[14] M. Leconte, J. Martin, N. Rakotomalala, and D. Salin, Phys. Rev. Lett. **90**, 128302 (2003).

[15] C. R. Nugent, W. M. Quarles, and T. H. Solomon, Phys. Rev. Lett. **93**, 218301 (2004).

[16] M. S. Paoletti and T. H. Solomon, Europhys. Lett. **69**, 819 (2005).

[17] H. Aref, J. Fluid Mech. **143**, 1 (1984).

[18] J. M. Ottino, *The Kinematics of Mixing: Stretching, Chaos and Transport* (Cambridge University Press, Cambridge, 1989).

[19] E. R. Abraham, Nature (London) **391**, 577 (1998).

[20] E. R. Abraham, C. S. Law, P. W. Boyd, S. J. Lavender, M. T. Maldonado, and A. R. Bowie, Nature (London) **407**, 727 (2000).

[21] O. Kupervasser, Z. Olami, and I. Procaccia, Phys. Rev. E **59**, 2587 (1999).

[22] F. A. Williams, *Combustion Theory* (Benjamin-Cummings, New York, 1985).

[23] M. N. Kuperman and H. S. Wio, Physica A **272**, 206 (1999).

[24] T. H. Solomon and J. P. Gollub, Phys. Rev. A **38**, 6280 (1988a).

[25] T. H. Solomon, S. Tomas, and J. L. Warner, Phys. Rev. Lett. **77**, 2682 (1996).

[26] T. H. Solomon, S. Tomas, and J. L. Warner, Phys. Fluids **10**, 342 (1998).

[27] A. I. Olemskoi and V. F. Klepikov, Phys. Rep. **338**, 571 (2000).

[28] A. L. Lin, A. Hagberg, E. Meron, and H. L. Swinney, Phys. Rev. E **69**, 066217 (2004).

[29] J. Xin, SIAM Rev. **42**, 161 (2000).

[30] A. N. Kolmogorov, I. G. Petrovskii, and N. S. Piskunov, Moscow Univ. Math. Bull. (Engl. Transl.) **1**, 1 (1937).

[31] R. A. Fisher, Proc. Annu. Symp. Eugen. Soc. **7**, 355 (1937).

[32] L. Kuhnert and H.-J. Krug, J. Phys. Chem. **91**, 730 (1987).

[33] A. J. Majda and P. R. Kramer, Phys. Rep. **314**, 237 (1999).

[34] A. C. Marti, F. Sagues, and J. M. Sancho, Phys. Fluids **9**, 3851 (1997).

[35] P. D. Ronney, in *Modeling in Combustion Science*, edited by J.

Buckmaster and T. Takeno (Springer-Verlag, Berlin, 1994), pp. 3–22.

[36] A. R. Kerstein, W. T. Ashurst, and F. A. Williams, Phys. Rev. A **37**, 2728 (1988).

[37] S. Chandresekhar, *Hydrodynamic and Hydromagnetic Stability* (Clarendon, Oxford, 1961).

[38] B. Shraiman, Phys. Rev. A **36**, 1374 (1987).

[39] T. Solomon and J. Gollub, Phys. Fluids **31**, 1372 (1988b).

[40] P. Castiglione, A. Crisanti, A. Mazzino, M. Vergassola, and A. Vulpiani, J. Phys. A **31**, 7197 (1998).

[41] T. H. Solomon, A. T. Lee, and M. A. Fogleman, Physica D **157**, 40 (2001).

[42] R. Camassa and S. Wiggins, Phys. Rev. A **43**, 774 (1991).

[43] L. Glass, Nature (London) **410**, 277 (2001).

[44] W. J. Yeah, D. R. He, and Y. H. Kao, Phys. Rev. Lett. **52**, 480 (1984).

[45] A. L. Lin, M. Bertram, K. Martinez, and H. L. Swinney, Phys. Rev. Lett. **84**, 4240 (2000).

[46] V. I. Arnold, Trans. Am. Math. Soc. **46**, 213 (1965).

[47] T. H. Solomon and I. Mezić, Nature (London) **425**, 376 (2003).

[48] H. Willaime, O. Cardoso, and P. Tabeling, Phys. Rev. E **48**, 288 (1993).

[49] V. Pérez-Villar, A. P. Munuzuri, and V. Pérez-Munuzuri, Phys. Rev. E **61**, 3771 (2000).

[50] R. J. Field and M. Burger, *Oscillations and Traveling Waves in Chemical Systems* (Wiley, New York, 1985).

[51] S. K. Scott, *Oscillations, Waves, and Chaos in Chemical Kinetics* (Oxford University Press, Oxford, 1994).

[52] V. Gaspar, G. Basza, and M. T. Beck, Z. Phys. Chem. (Leipzig) **264**, 43 (1983).

[53] M. K. R. Reddy, Z. Nagy-Ungvarai, and S. C. Muller, J. Phys. Chem. **98**, 12255 (1994).

[54] T. Sakurai, E. Mihaliuk, F. Chirila, and K. Showalter, Science **296**, 2009 (2002).

[55] M. S. Paoletti, Honors thesis, Bucknell University, 2005, contact tsolomon@bucknell.edu for a copy.

[56] M. H. Jensen, P. Bak, and T. Bohr, Phys. Rev. A **30**, 1960 (1984).

[57] A nearly-saturated solution of $[Ru(bpy)_3]Cl_2$ is produced by dissolving 4.866 g of the solid $[Ru(bpy)_3]Cl_2 6H_2O$ in 65 mL of distilled water. To this solution, 31 mL of 0.4272 M $AgNO_3$ is added dropwise to the $[Ru(bpy)_3]Cl_2$ solution and stirred. The Ag^+ ions from the $AgNO_3$ combine with the Cl^- ions from the ruthenium indicator to form $AgCl$, which is insoluble in water and forms a precipitate. The precipitate is filtered several times until it has been completely removed. Once the $AgCl$ precipitate has been completely removed, there is still a small excess of Ag^+ ions left in the solution. The Ag^+ could cause spontaneous Ru^{3+} production during the experiment, so the excess Ag^+ must also be removed. Once again, a single-replacement technique is employed; $NaBr$ is used to remove the excess Ag^+ ions by the precipitation of $AgBr$. A solution of $NaBr$ is prepared by dissolving 0.10 g of solid $NaBr$ in 10 mL of distilled water. Approximately 4 mL of this solution is added dropwise and $AgBr$ precipitate forms. The precipitate is completely filtered. To ensure that the maximum number of Ag^+ ions have been removed, a few drops of the $NaBr$ are added to see if further precipitation occurs. If precipitate does form then $NaBr$ is added dropwise until no further precipitate forms. This process is repeated until the excess Ag^+ ions and precipitate have been removed. The resulting solution is approximately 65 mM $[Ru(bpy)_3]^{2+}$.